Optical properties of thin semicontinuous gold films over a wavelength range of 2.5 to 500 μm

Yoad Yagil
Department of Physics and Astronomy, Raymond and Beverly Sackler Faculty of Exact Sciences, Tel-Aviv University, 69978 Tel-Aviv, Israel

Patrice Gadenne
Laboratoire de Optique des Solides, Universite Pierre et Marie Curie, 4 place Jussieu, 75230 Paris CEDEX 05, France

Christian Julien
Laboratoire de Physique des Solides, Universite Pierre et Marie Curie, 4 place Jussieu, 75230 Paris CEDEX 05, France

Guy Deutscher
Department of Physics and Astronomy, Raymond and Beverly Sackler Faculty of Exact Sciences, Tel-Aviv University, 69978 Tel-Aviv, Israel
(Received 3 December 1991)

The optical reflectance and transmittance of percolating gold films close to the metal-insulator transition were measured over an extended wavelength range: from 2.5 to 500 μm. It is shown that the inhomogeneous nature of such films controls the optical properties even at such long wavelengths as 500 μm, where the typical grain size is 10 nm. Effective-medium theory is shown to be invalid close to the percolation threshold even at 500 μm. Comparison of the measured data of all the samples with the scaling model of Y. Yagil *et al.* [Phys. Rev. B **43**, 11 342 (1991)] yields excellent agreement over the entire wavelength range. In particular, the short length scale determined by the anomalous diffusion relation is shown to be the relevant length scale for the optical measurements. This scaling model for the optical properties of such films is thus experimentally justified, both qualitatively and quantitatively.

INTRODUCTION

The optical properties of composite materials have been widely investigated, both theoretically and experimentally. For the metal-insulator composites an anomalous absorption peak is found in the visible or near-infrared regime, resulting from the Maxwell-Garnett dipole-dipole resonance (see, for example, Ref. 1). Several effective-medium theories have been used to calculate the optical properties of such materials, where the simplest ones are the Maxwell-Garnett,[2] the Bruggeman,[3] and modifications of these two approaches.[4] It has been found that these theories are applicable if the samples are not too close to the metal-insulator transition and the optical wavelength is long enough, i.e., as long as the optical wavelength is much larger than the metallic grains.[1,5-7] Recently, a new scaling model was suggested[8] calculating the optical properties of two-dimensional composites near the percolation threshold (the metal-insulator transition). In this model the relevant length scale $L(\omega)$ is the anomalous diffusion length[9] on the time scale $1/\omega$ (ω is the optical frequency) and is much shorter than the optical wavelength. As long as the percolation correlation length ξ is larger than $L(\omega)$, the film is inhomogeneous and the effective-medium approach is not applicable. Only when $L(\omega)$ is much larger than ξ can the film be treated as a homogeneous medium. Following the above arguments, films close to the percolation threshold may appear inhomogeneous even in the far-infrared regime, where ξ is much shorter than the optical wavelength but larger than $L(\omega)$. The test of this prediction is the goal of this work.

In situ optical measurements[10] have shown that such films should be considered as inhomogeneous over a wide range below and above the percolation threshold at a wavelength of 2.2 μm. Much longer wavelengths should thus be used in order to detect the crossover from inhomogeneous to homogeneous behavior. Measurements over an extended wavelength regime (2.5–500 μm) were done, using three types of spectrometers, to study the optical properties of semicontinuous gold films close to the percolation threshold. The measured data are compared with the effective-medium theory and with the scaling model. The results verify the scaling approach and show that the anomalous diffusion length is indeed the relevant length scale.

EXPERIMENT

Samples of various average thicknesses were evaporated on glass or on silicon substrates in a vacuum of 2×10^{-6} Torr. The sheet resistance R_s of each sample was measured immediately after removal from the vacuum chamber. Since the same evaporation conditions were repeated very carefully on each run, and because we are in the percolating regime, the average mass thickness d can be taken as proportional to the surface coverage parameter p.[10] This relation yields a power-law dependence between R_s and the average mass thickness d, as shown in Fig. 1. Four samples (denoted here as A, B, C,

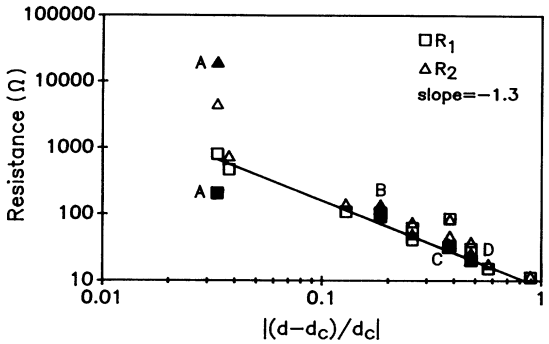

FIG. 1. A log-log plot of the measured sheet resistance of all the samples vs the absolute value of the normalized thickness parameter $|d-d_c|/d_c$, $d_c=6.8$ nm. The measured resistance immediately after the evaporation is indicated by squares (R_1 in Table I) and the resistance before the optical measurements by triangles (R_2 in Table I). The silicon substrate samples are indicated by filled squares and triangles. Note that the silicon and glass substrate samples fit the same power law [$R \propto (d-d_c)^{\mu}$] with the same value for d_c (the linear fit is sensitive to d_c but not to the exact value of μ). This behavior indicates that the microgeometry of the Au film on both substrates is identical, as both d_c and p_c are sensitive to the exact microgeometry.

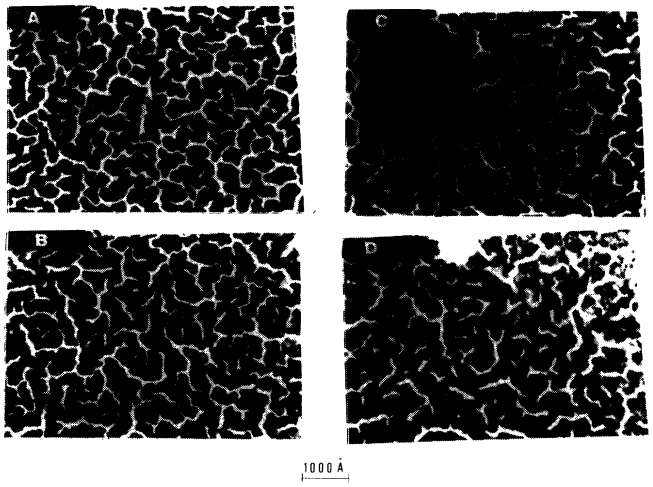

FIG. 2. TEM micrographs of samples $A-D$.

and D) were evaporated on silicon substrates, transparent for wavelengths larger than 2 μm.[11] Normally, both the average mass thickness at the percolation threshold, d_c, and the critical surface coverage value p_c, are sensitive to the exact microgeometry. Films evaporated on different substrates are thus expected to yield different values of these two quantities, and will not fit the same linear line on a log-log plot. In contrast, both the silicon and the glass substrate samples are described by *the same* power law, as shown in Fig. 1. We conclude that the film growth is identical on glass and on silicon substrates, probably due to the oxide layer of the silicon substrate [a naturally SiO_2 layer is formed with a typical thickness of 2 nm (Ref. 12)].

Reflectance and transmittance measurements were done with three different spectrophotometers: Cary-17 for the visible and infrared (IR) regime (up to 2.7 μm), Perkin-Elmer 580B for the 2.5–25-μm region, and a Bruker IFS 113V Fourier transform spectrometer (FFT) for the far-infrared (FIR) measurements (17–500 μm). The absolute accuracy of the above spectrometers are 1%, 2%, and 5–10%, respectively. The optical measurements were done a couple of months after the samples were prepared. The sheet resistance of all the samples had changed during this period, as listed in Table I and shown in Fig. 1. Note that a couple of samples, very close to the percolation threshold, underwent a transition from metallic to insulating. This behavior is common to such films, i.e., they are unstable when removed from the vacuum chamber, and may show slow variations with time. After completion of all electrical and optical measurements, the "silicon" samples were covered by a thin carbon layer and removed from the silicon substrate by a chemical method. Figure 2 shows the TEM (transmis-

TABLE I. Summary of the data of all the samples: average mass thickness d (nm), measured resistance immediately after removal from the vacuum chamber, R_1, and measured resistance just before the optical measurements, R_2. The critical mass thickness at the percolation threshold is $d_c=6.8$ nm.

Sample	d	$\frac{d-d_c}{d_c}$	$\frac{R_1}{sqr}$	$\frac{R_2}{sqr}$
1	1.35	−0.800		
2	2.65	−0.608		
3	4.03	−0.403		
4	4.70	−0.303		
5	4.88	−0.277		
6	5.35	−0.207		
7	6.00	−0.111		
8	6.47	−0.042	1 240 000	
9	7.03	0.041	800.0	3 620.0
10(A)	7.03	0.041	205.0	19 500.0
11	7.06	0.045	466.0	600.0
12	7.67	0.137	108.0	114.0
13	8.06	0.193	92.0	94.8
14(B)	8.06	0.193	101.0	116.0
15	8.06	0.193	105.0	110.6
16	8.56	0.267	41.2	39.6
17	8.56	0.267	62.0	60.0
18(C)	9.38	0.389	32.0	35.7
19	9.41	0.394	85.2	67.2
20	9.41	0.394	33.6	37.6
21	10.05	0.490	30.0	30.4
22(D)	10.05	0.490	20.2	25.6
23	10.70	0.585	15.2	14.2
24	12.88	0.908	11.2	9.5
25	15.02	1.226	6.8	6.6
26	15.02	1.226	5.2	4.6
27	18.23	1.700	3.6	3.3
28	21.46	2.180	2.8	2.6
29	24.99	2.702	2.4	2.0

sion electron microscope) micrographs of these samples. One can easily see that samples C and D are well above the percolation threshold p_c, sample B is metallic and much closer to it, and sample A is very close to p_c, the percolation correlation length ξ is larger than the size of the picture, hence from the TEM micrograph it is not clear if it is metallic or insulating. These micrographs were digitized and the surface coverage parameter p of each sample was calculated. The results were compared to the average mass thickness d and show a linear dependence, as expected ($p=0.66, 0.74, 0.80, 0.84$, $d=7.03, 8.06, 9.38, 10.05$ nm for samples A, B, C, and D, respectively).

Transmittance (T) measurements in both the Cary-17 and the Perkin-Elmer spectrometers were done with a clean substrate in the reference beam. The glass substrate samples were cut in two pieces, the one without a metallic film being used in the reference beam. This procedure ensures the absence of differences between the actual substrate and the reference one, which is most important in the 2.5–5-μm regime, where the glass substrate is highly absorbing. Reflectance (R) measurements were done using a special V-W adapter, where the light beam passes the sample twice, obtaining R^2. In order to have enough sensitivity for low reflectance, we have used an aluminum mirror for one of the two reflection paths, obtaining RR_{Al} rather than R^2 (R^2_{Al} was measured in the same way). The same V-W adapter was used in both the Cary-17 and the Perkin-Elmer 580B spectrometers, enabling accurate calibration of the Perkin-Elmer data by those of the Cary-17. These results are all summarized in Fig. 3.

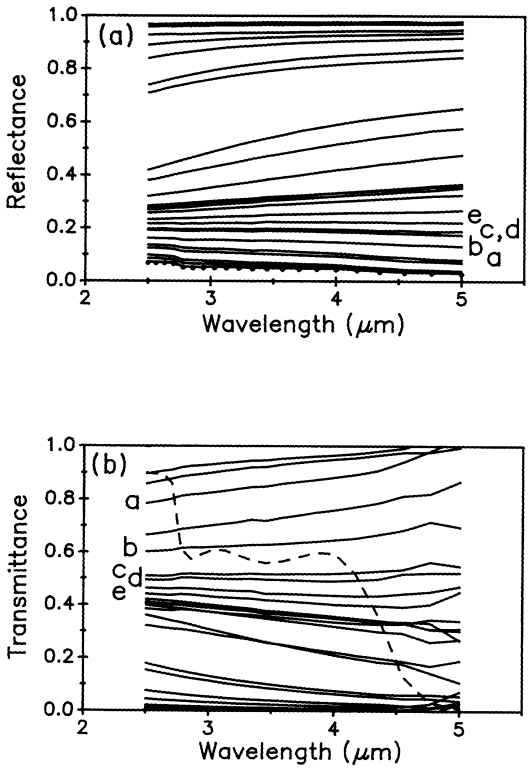

FIG. 3. Optical results of all the samples evaporated on glass substrate. (a) Reflectance. (b) Transmittance $-T/T_0$, where T_0 is the transmittance of the glass substrate. The transmittance of the glass itself is indicated by a dashed line and its reflectance by dots. The marked curves are for the following samples: a, 6; b, 7; c, 8; d, 11; e, 12.

The Bruker FFT spectrometer has already been well described.[13–15] It works under vacuum, in order to avoid the water absorption which is significant in the FIR regime. This apparatus is mainly built as a Michelson interferometer in the Genzel configuration.[16,17] The optical path difference δ is accurately determined by monitoring the interferogram using the monochromatic wave of a He-Ne laser. The large wavelength range scanned here requires several modifications of the interferometer i.e., light source, beamsplitter, and detector. These are automatically performed by the specially dedicated computer. We have separated the wavelength range into two parts: up to 20 μm we have used a HCT (He-Cd-Te) detector cooled at 77 K, together with a Ge/KBr beamsplitter and a Globar light source. For the 20–500-μm regime, we have used a germanium Bolometer cooled at 4.2 K with a special bandpass filter, a 6-μm-thick Mylar beamsplitter, and a Hg L light source. Reflectance measurements were performed using a reflection unit, operating at an angle of incidence of 11°. This is slightly different from the 4° V-W reflecting setup used on both the Cary-17 and the Perkin-Elmer 580B spectrometers. Each spectrum represented in the experimental results is an average over 100 scans recorded with a spectral resolution of 0.5 cm^{-1}. The raw spectra exhibited well-defined oscillations due to interference between the waves reflected by the two faces of the thin silicon substrate (300 μm). These oscillations were smoothed out by numerical filtering.

In order to calibrate our FIR measurements as accurately as possible, we have calibrated the FFT data to those of the Cary-17 and the Perkin-Elmer 580B spectrometers. On the FFT spectrometer, absolute values of the transmittance are obtained after taking into account the transmittance measurements of a bare silicon substrate and of an empty aperture. In contrast, the reflectance measurements are not absolute: they have to be compared to, and calibrated by using a well-known sample. For this purpose, we have used a bulk optically polished gold mirror, over the whole wavelength range. Finally we have adjusted the data of the Perkin-Elmer to that of the Cary-17 at 2.5 μm and the data of the FFT to the modified Perkin-Elmer data in the range 17–25 μm. Taking into account all the steps of the measurements and calibration, we obtain an overall accuracy of 1–2 % in the 3–30-μm regime for both R and T. For the 30–500-μm range, the reflectance data accuracy is of the order of 5–6 % while the transmittance accuracy is of the order of 3%.

RESULTS

The measured reflectance R and transmittance T of the Au films evaporated on glass substrates are shown if Fig. 3, where the transmittance of one of the glass substrates

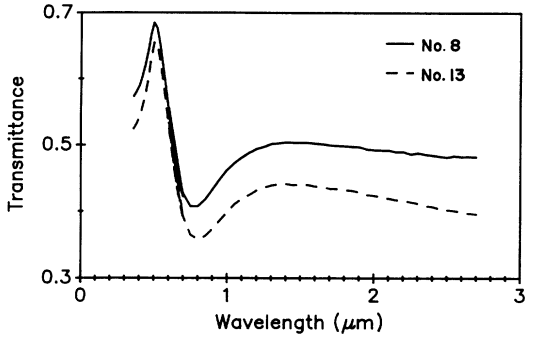

FIG. 4. Transmittance of two samples from 0.3 to 2.7 μm. The absorption peak at 0.8 μm is due to the Maxwell-Garnett resonance. The data indicate that above 1.5 μm the existence of this resonance is unimportant.

is shown by a dashed line. These measurements are limited to 5 μm as the glass substrate is opaque beyond this wavelength. The reflectance R has an intermediate value and is almost wavelength independent close to the percolation threshold p_c. R is high and increases with increasing wavelength for conducting samples and is low and decreases with increasing wavelength for the insulating ones. The transmittance data T/T_0, where T_0 is the transmittance of the glass substrate, shows the same general behavior: intermediate values and weak wavelength dependence close to p_c, low value and decrease with increasing wavelength for the conducting samples, and the opposite trend for the insulating ones. Such a behavior was detected at shorter wavelengths (normally up to 2.5 μm) and interpreted by the inhomogeneity of the samples at length scales shorter than the percolation correlation length.[6,18–22] Observation of such a broadened transition region from metallic to dielectric behavior at 5 μm indicates that the relevant length scale is much shorter than the optical wavelength. The Maxwell-Garnett resonance for these films is at about 0.8 μm and its effect may be neglected above 1.5 μm as shown in Fig. 4.

Optical measurements beyond 5 μm were done on films evaporated on silicon substrate, which is transparent in the far-infrared regime. The measured reflectance and transmittance of films $A-D$ as well as that of the silicon substrate are shown in Fig. 5. Films C and D show a clear metallic behavior, i.e., a high reflectance and a very low transmittance at the long wavelengths. Film B shows a much higher transmittance and lower reflectance, but can still be determined as a metallic film with poor conductivity (i.e., the long-wavelength response is well described by its dc conductivity, using the Drude formula). The optical response of film A seems to be insulatorlike, since the reflectance is relatively low and the transmittance approaches that of the substrate for very long wavelength. Analysis of the optical properties of these films requires the separation of the contributions of the gold film and the silicon substrate. For a homogeneous

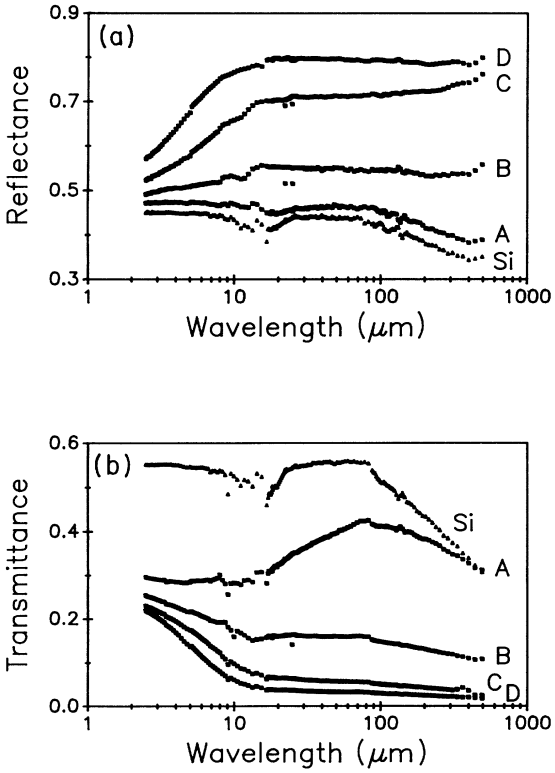

FIG. 5. Reflectance (a) and transmittance (b) of samples $A-D$ and of the silicon substrate, over the entire wavelength range 2.5–500 μm. Note that the wavelength axis is logarithmic.

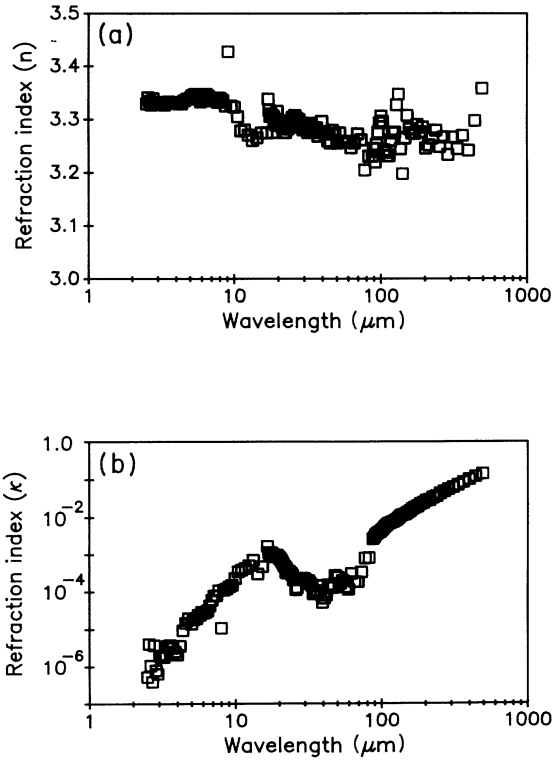

FIG. 6. The complex refractive index $\bar{n}=n+i\kappa$ of the silicon substrate as measured by us. (a) The real part n, (b) the imaginary part κ (logarithmic scale).

film, the effective complex dielectric constant may be deduced from the above data. In our case, however, the films cannot be treated as homogeneous[8,10] and such a separation is not allowed. We thus have calculated the complex refractive index $\bar{n}=n+i\kappa$ of the silicon using our measurements on a bar substrate. We then have used these values to calculate the optical response of the film on the substrate, in terms of the effective-medium theory (EMT) and the scaling model. These can be directly compared to the measured quantities. The measured refractive index of the silicon substrate is shown in Fig. 6. For the real part we find a fairly constant value over the entire wavelength range $n \simeq 3.3$, very close to the values listed in the literature.[11] The imaginary part, κ, is wavelength dependent as shown in Fig. 6(b). The extra structure above 10 μm results from interaction with phonons.[23]

EFFECTIVE-MEDIUM APPROACH

The effective-medium approach assumes that the film can be treated as homogeneous at the relevant length scale, hence the inhomogeneous nature is smeared out. For a homogeneous media, the inverse wave number $k^{-1}=\lambda/2\pi$ is the relevant length scale, which is of the order of tens of micrometers in the FIR regime. One would expect percolating films with typical grain size of 10 nm to be homogeneous on such length scales. We thus have tried to fit the optical data to the modified Bruggeman EMT (Refs. 3 and 1), which is the more relevant one close to the percolation threshold. In this model, two components with dielectric constants ϵ_m and ϵ_i and volume fractions p and $(1-p)$, respectively, are assumed to be present as small ellipsoids embedded in the supposedly uniform effective medium. The condition that the total dipole moment induced in these ellipsoids vanishes leads to the equation

$$p\frac{\epsilon_m-\epsilon_{\text{eff}}}{g\epsilon_m+(1-g)\epsilon_{\text{eff}}}+(1-p)\frac{\epsilon_i-\epsilon_{\text{eff}}}{g\epsilon_i+(1-g)\epsilon_{\text{eff}}}=0\ , \quad (1)$$

where g is the depolarization factor of the ellipsoidal grains ($g=\frac{1}{3}$ for spheres). This model has four parameters: ϵ_i, ϵ_m, p, and g. The metal-insulator transition in this model is at $p=g$ thus $g=p_c=0.68$ as estimated from the TEM micrographs. The surface coverage p is again given by the TEM analysis, however, we allowed some variations of this quantity for better fitting. In the FIR regime, the metal behaves like Drude's free electron gas, and we can use $\epsilon_m=\epsilon_0+i4\pi\sigma_{\text{dc}}/(1-i\omega\tau)$, where σ_{dc} is determined from the optical properties of samples C and D at long wavelengths, and τ served as a fitting parameter at short wavelengths. For better fitting we have used Theye's formula[24] for the frequency dependence of the relaxation time $\tau^{-1}=\tau_0^{-1}+b_\tau\omega^2$, where b_τ is another fitting parameter. It should be emphasized that the value of τ affects only the short wavelengths, and the optical properties at the long wavelengths depend mostly on σ_{dc} and p. The calculated reflectance and transmittance *including* the silicon substrate are shown in Fig. 7 and the parameters used for each sample are given in the Appendix. The optical properties of samples C and D are well described by the EMT calculation, except that they present some discrepancies at the short wavelengths. For sample B, good agreement with the measured values is achieved by artificially reducing the surface coverage parameter p from 0.74 down to 0.715 or $(p-p_c)$ is 0.035 instead of 0.06. However, this result shows that the critical region of the percolation transition in the EMT picture is too narrow, as was shown in Ref. 8. For sample A we could not fit the experimental data using the EMT approach. The family of curves for various values of p close to p_c show that film A behaves as a more metallic film at short wavelengths and as an insulating one at longer wavelengths, hence it cannot be described by the effective-medium approach. This film is the most inhomogeneous one and its percolation correlation length ξ is the largest. The disagreement at such long wavelengths suggests that the relevant length scale in this case is much shorter than k^{-1}, as ξ is of the order of a few micrometers. We conclude this section by emphasizing that very close to p_c effective-medium theory is not valid at any optical wavelength.

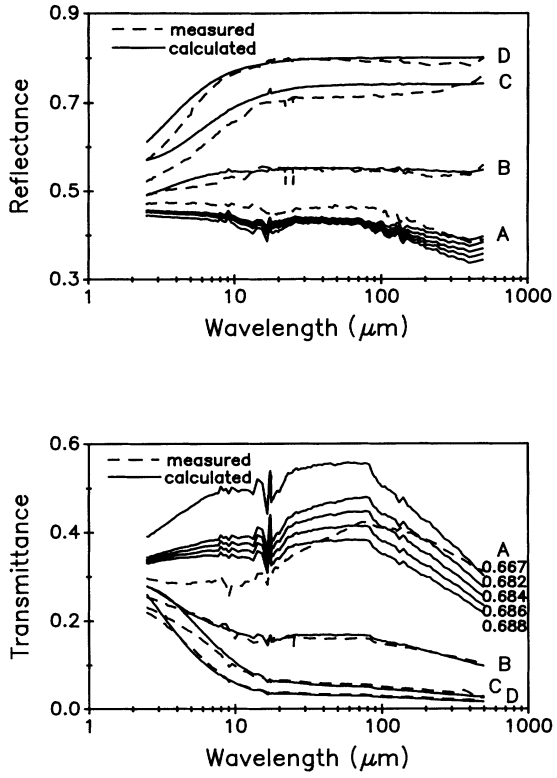

FIG. 7. Fitting of the measured data by the EMT method (full lines) for samples A–D. The measured data are shown by dashed lines. The fitting parameters are given in the Appendix. For sample A fitting by EMT is impossible as illustrated by a family of graphs of various surface coverage parameter p (indicated in the graph; $p_c=0.68$). The extra structure of the transmittance curves at the wavelengths 15–20 μm is due to the silicon substrate.

SCALING APPROACH

Recently a scaling based model was suggested for the optical properties of semicontinuous two-dimensional (2D) metal films.[8] The outlines of this approach are the following: (1) The effective dielectric constant has no physical meaning close to p_c. Moreover, one has to average the reflectance and transmittance on different areas, where the film have different contributions. (2) The local optical response is deduced from the local complex ac conductivity on the relevant length scale. This quantity is described by a bimodel distribution function, taking into account the ac conductivity of the metallic grains and the intercluster capacitance. (3) The relevant length scale is much shorter than the optical wavelength and is given by the anomalous diffusion relation[9] $L(\omega)=L_0(1/k\xi_0)^{1/(2+\theta)}$, where k is the wave number, $\theta\simeq 0.8$ for 2D, L_0 is a coefficient of the order of unity, and ξ_0 is the basic scale of the percolation correlation length $\xi=[(p-p_c)/p_c]^{-\nu}$. Both L and ξ are measured in units of ξ_0. The two basic conductivities entering the model for a semicontinuous metal film are given by

$$\sigma_1=\sigma_{\rm dc}/(1-i\omega\tau)\ , \tag{2a}$$

$$\sigma_2=-i\omega C_0\ , \tag{2b}$$

where C_0 is the capacitance between two adjacent metallic grains. The total ac conductivity of a square of linear size $L\ll\xi$ is given by the scaling function[25]

$$\sigma(L)=\sigma_1 L^{-\mu/\nu}F((\sigma_1/\sigma_2)L^{(\mu+s)/\nu})\ . \tag{3}$$

The ac conductivity of a "metallic" square is thus given by

$$\sigma_m(L)=\frac{A_1\sigma_{\rm dc}}{1+\omega^2\tau^2}L^{-\mu/\nu}+i\left[\frac{A_1\sigma_{\rm dc}\omega\tau}{1+\omega^2\tau^2}L^{-\mu/\nu}-A_2C_0\omega L^{s/\nu}\right],\quad L(\omega)\ll\xi\ , \tag{4a}$$

$$\sigma_m(L)=\sigma_m(\xi),\quad L(\omega)\gg\xi \tag{4b}$$

and for a "dielectric" square (zero dc conductivity):

$$\sigma_i(L)=\frac{A_3\omega^2C_0^2}{\sigma_{\rm dc}}L^{(\mu+2s)/\nu}+i\left[\frac{A_3\omega^2C_0^2\omega\tau}{\sigma_{\rm dc}}L^{(\mu+2s)/\nu}-A_4C_0\omega L^{s/\nu}\right],\quad L(\omega)\ll\xi \tag{5a}$$

$$\sigma_i(L)=\sigma_i(\xi),\quad L(\omega)\gg\xi\ , \tag{5b}$$

where $L=L(\omega)$ if $L(\omega)\ll\xi$ and $L=\xi$ at the opposite limit. The local dielectric constant is given by the usual relation $\epsilon=\epsilon_0+i4\pi\sigma/\omega$, and the optical response of each square of linear size L may then be calculated. Essentially there are no fitting parameters in this model, however, the values of some physical parameters are unknown. We have thus used the parameters of Ref. 8 with several changes. $\sigma_{\rm dc}$ was adjusted to recover the optical response of films C and D at long wavelengths, where the scaling model reduces to a Drude metal with reduced dc conductivity. The optical relaxation time $\tau^{-1}=\tau_0^{-1}+b_\tau\omega^2$ was adjusted for each film to fit the short-wavelengths response. $\xi_0=10$ nm, which is the average grain size and fits the short-wavelength behavior of films $A-C$. The full parameter listings of both the EMT and the scaling model calculations are given in the Appendix. The calculated reflectance and transmittance are shown in Fig. 8 where the data include the silicon substrate contributions as measured (see Fig. 6). The calculated curves fit the measured data within 2–3 % for all films and at all wavelengths, i.e., well within the experimental uncertainty.

The crossover from inhomogeneous to homogeneous behavior does occur at the wavelength $\lambda_\xi=2\pi\xi_0(\xi/L_0)^{2+\theta}$ where $L(\omega)=\xi$. The values of λ_ξ for samples C and D (see the Appendix) show that they should be treated as homogeneous films over the entire measured range, thus the scaling model reduces to the effective-medium description. However, at short wavelengths this model yields better agreement with the measured values than the EMT ones. This difference will be discussed later. For film B, $\lambda_\xi=10.6$ μm hence EMT is not valid in this range and at shorter wavelengths. As discussed above, the optical properties of film B could be calculated using the EMT approach only if $(p-p_c)$ is reduced by a factor of 2.

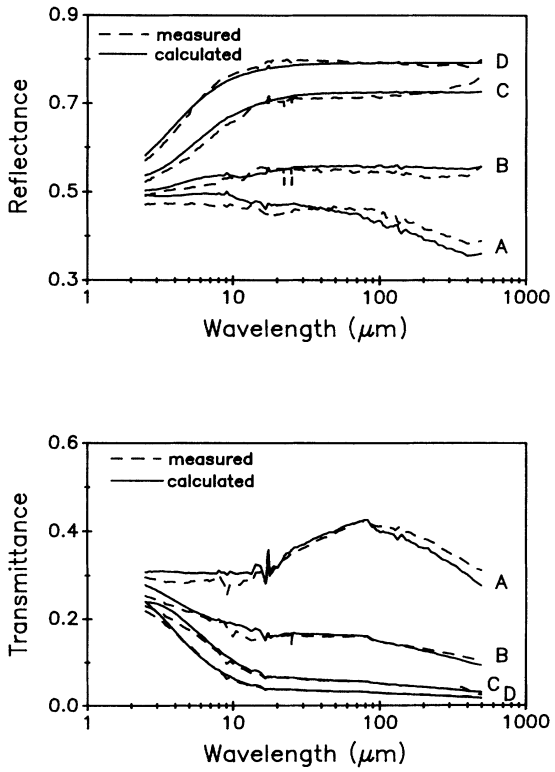

FIG. 8. Fitting of the measured data by the Scaling model (full lines) for samples $A-D$. The measured data are shown by dashed lines. The fitting parameters are given in the Appendix. The extra structure of the transmittance curves at the wavelengths 15–20 μm is due to the silicon substrate.

The most important result is that of film A which is slightly below the percolation threshold. In this case the EMT approach cannot yield any optical response which is close to the measured data while the scaling model does. For film A, λ_ξ is larger than 500 μm, the film is predicted to be inhomogeneous over the entire measured regime, and the effective dielectric constant is meaningless at all wavelengths. The agreement between the scaling model and the measured data shows that the relevant length scale is indeed much shorter than the optical wavelength and the anomalous diffusion assumption is verified.

DISCUSSION

The calculated reflectance, transmittance, and absorptance of films $A-D$ *without the silicon substrate effect* are shown in Fig. 9. The data are determined using both the EMT and the scaling calculations, as described above, where the silicon substrate is replaced by vacuum, i.e., a "substrate" with $\epsilon=1$. For film A, these two models yield a totally different response as has been discussed in the previous sections, where EMT was shown to fail. The scaling model yields a large absorptance, slowly decreasing with increasing wavelength. This optical response shows, experimentally, the shortness of $L(\omega)$ compared to the inverse wave number $k^{-1}=\lambda/2\pi$. For film A, $\xi\simeq 2$ μm hence $k\xi\simeq 1$ at $\lambda\simeq 10$ μm where $L(\omega)/\xi\simeq 1$ at $\lambda>500$ μm. The optical response of this film confirms, experimentally, that $L(\omega)$ is indeed the relevant length scale.

The EMT and scaling responses of films $B-D$ are similar in the long-wavelength regime ($\lambda>10$ μm). At shorter wavelengths, EMT yields a slow decrease in the optical absorptance with decreasing wavelength, while the scaling model yields an increase for films C and D, and a decrease for film B. Films C and D are supposed to be well described by the EMT approach even at these wavelengths, hence it is interesting to understand the origin of these differences. In the limit where $L(\omega)$ is not much larger than ξ, and for $p>p_c$, the scaling model yields a distribution of metallic conductances, which becomes narrower as $[\xi/L(\omega)]$ decreases. If the average conductance is relatively high (i.e., yields a low absorptance), the absorption is enhanced by the distribution of the local conductances. Such a distribution is, of course, absent in the EMT approach and may thus explain the differences in the short-wavelength regime. Enhancement of the optical absorptance results also from the intercluster and intracluster capacitance. This effect is not included in the EMT calculation used here. The importance of the conductance distribution and of the capacitance depends on the optical wavelength and on $\Delta p=(p-p_c)/p_c$. The capacitance becomes important when [see Eq. (4)]

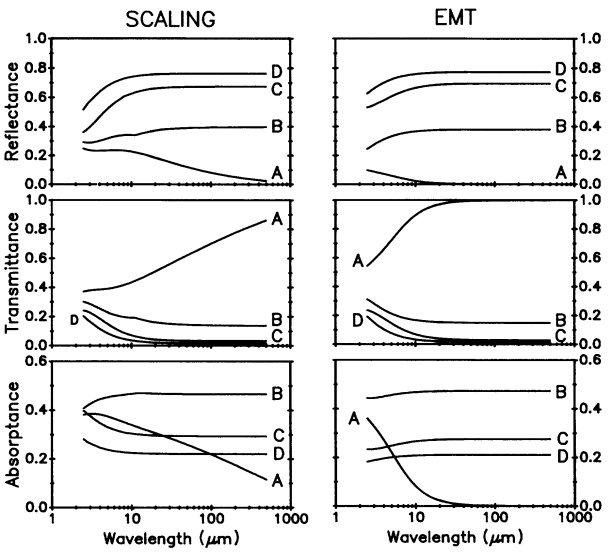

FIG. 9. Reflectance, transmittance, and absorptance of films $A-D$ without the silicon substrate effect, as calculated by the scaling and the EMT models. The complete set of parameters is given in the Appendix. Film A is calculated with $p=0.667$ in both models. Note the difference between the two models in the short-wavelength regime for films $B-D$.

$$A_2 C_0 \omega \xi^{s/\nu} \simeq A_1 \sigma_{dc} \frac{\omega\tau}{1+\omega^2\tau^2} \xi^{-\mu/\nu} . \tag{6}$$

For a fixed wavelength, one may define a threshold concentration Δp_{cp} above which the capacitance may be neglected. Replacing ξ by $\Delta p_{cp}^{-1/\nu}$ yields

$$\Delta p_{cp} = \left\{ \frac{A_2}{A_1} \frac{C_0}{\tau\sigma_{dc}} \left[1 + \left[\frac{2\pi c\tau}{\lambda} \right]^2 \right] \right\}^{1/(\mu+s)} . \tag{7}$$

Capacitance effects are thus important if $\Delta p < \Delta p_{cp}$.

The conductance distribution is broadened if $L(\omega)<\xi$. For $L(\omega)>\xi$ this distribution decays as $[\xi/L(\omega)]^2$. For a fixed wavelength, the threshold concentration Δp_d is thus given by

$$\Delta p_d = L_0^{-1/\nu} \left[\frac{2\pi\xi_0}{\lambda} \right]^{1/[\nu(2+\theta)]} , \tag{8}$$

i.e., for $\Delta p > \Delta p_d$ the distribution decays rapidly.

The wavelength dependence of Δp_{cp} is stronger than that of Δp_d: $\Delta p_{cp} \propto \lambda^{-2/(\mu+s)} \simeq \lambda^{-1/1.3}$ while $\Delta p_d \propto \lambda^{-1/[\nu(2+\theta)]} \simeq \lambda^{-1/3.7}$. One can define a crossover wavelength λ_{CO}, where $\Delta p_{cp}=\Delta p_d$. Assuming $\omega\tau \gg 1$:

$$\lambda_{CO1} = 2\pi\xi_0 \left[\frac{A_1}{A_2} \frac{\sigma_{dc}}{C_0} \frac{\xi_0^2}{\tau c^2 L_0^{(\mu+s)/\nu}} \right]^{-[\nu(2+\theta)]/[2\nu(2+\theta)-(\mu+s)]} \tag{9}$$

while for $\omega\tau \ll 1$ we get

$$\lambda_{CO2}=2\pi\xi_0\left[\frac{A_1}{A_2}\frac{\sigma_{dc}}{C_0}\frac{\tau}{L_0^{(\mu+s)/\nu}}\right]^{[\nu(2+\theta)]/(\mu+s)} . \quad (10)$$

Estimating the above quantities (using $\mu=s=1.3$, $\theta=0.8$, and $\tau=5\times10^{-15}$) yields $\lambda_{CO1}\simeq2.6$ μm, $\Delta p_{CO1}=0.17$ ($\omega\tau\gg1$), hence $\lambda>\lambda_{CO1}$ over the entire measured wavelength regime. The long-wavelength crossover ($\omega\tau\ll1$) yields $\lambda_{CO2}\simeq85$ μm, $\Delta p_{CO2}=0.05$. In the range $\lambda_{CO1}<\lambda<\lambda_{CO2}$, both the capacitance and the conductance distributions are important for $\Delta p<\Delta p_{cp}(\lambda)$. The capacitance correction to the metallic conductance becomes less important as Δp increases, while the conductances are still distributed and the film is considered as inhomogeneous (note that the nonmetallic conductances are always dominated by the capacitance). If Δp is further increased, the film becomes homogeneous ($\Delta p>\Delta p_d$) and is well described by the EMT approach. In the two regimes $\lambda<\lambda_{CO1}$ and $\lambda>\lambda_{CO2}$, and for films with $\Delta p_d<p<\Delta p_{cp}$, capacitance effect dominates. In these regimes, the films may be considered as homogeneous, i.e., the effective-medium approach is valid, provided the capacitance is taken into account. For example, the optical properties are well described by $\sigma_m(\xi)$.

The capacitance effect criterion at wavelengths of 1 and 10 μm yields $\Delta p_{cp}(\lambda=1\ \mu\text{m})=0.3$ and $\Delta p_{cp}(\lambda=10\ \mu\text{m})=0.05$ (which is the lower limit of Δp_{cp}). For the conductance distribution, one finds $\Delta p_d(\lambda=1\ \mu\text{m})=0.17$ and $\Delta p_d(\lambda=10\ \mu\text{m})=0.1$. The normalized concentrations of samples A–D are $\Delta p(A)=-0.02$, $\Delta p(B)=0.09$, $\Delta p(C)=0.18$, and $\Delta p(D)=0.24$. For film C, $\Delta p(C)\simeq\Delta p_{CO1}$, hence at the short wavelengths (say 2.5–5 μm) both the capacitance and the conductance distributions have a significant effect. At longer wavelengths (up to 10 μm), the conductance distribution dominates, as Δp_{cp} decreases much more rapidly with increasing wavelength. This picture is true for film D as well, i.e., the enhanced absorption results mainly from the conductance distribution. It means that the optical properties of these two films will not show the excess absorptance should the capacitance effect be included in any effective-medium approach.

For film B, these two contributions are essential, as $\Delta p(B)<\Delta p_{CO1}$. In this case, the conductance distribution *decreases* the optical absorption because (a) the film is inhomogeneous for $\lambda<10$ μm, containing thus dielectric areas which have lower absorption, and (b) the average conductance of the metallic regions of film B yield a high absorptance, hence the distribution of metallic conductances introduces less absorbing metallic contributions.

In summary, the experimental results show unambiguously that geometrical details at length scales much shorter than the optical wavelength are crucial in the optical response of such films. It was shown that a set of films evaporated on glass substrates have a wide optical metal-insulator transition even at a wavelength of 5 μm. Moreover, we have shown that close to p_c effective-medium theory is not valid even at a wavelength as long as 500 μm, as in the case of film A. In contrast, the new scaling model[8] is shown to be accurate and powerful over the entire wavelength regime. The agreement between the measured reflectance and transmittance and the calculated ones is excellent for all samples over the entire range of wavelengths (see Fig. 8). The experimental verification of this model over such an extended wavelength regime shows that the relevant length scale is effectively determined by the anomalous diffusion relation, which was one of the main assumptions made in the above model. The shortness of this length scale is thus verified quantitatively as well as qualitatively. The optical response of film A, as well as the short-wavelength behavior of the more metallic films (especially film B) show the importance of the intercluster capacitance which was taken into account in the above model. We conclude that the new scaling model for the optical properties of percolating films is accurate and applicable. Experimental determination of the scaling functions used in this model, as well as the conductance distribution function and the crossover from inhomogeneous to homogeneous behavior can thus be done by optical measurements of such films or alternatively by microwave measurements on computer generated networks.

ACKNOWLEDGMENTS

This work was partially supported by the CNRS (Programme International de Cooperation Scientifique: "Milieux desordonnes denses"), by the U.S.-Israel Binational Science Foundation, and by the Oren Family Foundation.

APPENDIX

The parameters for the EMT and scaling calculations are, for EMT, $\sigma_{dc}=0.7\times10^{17}$ sec^{-1} (the bulk conductivity is 3.5×10^{17} sec^{-1}), $\epsilon_0=6.5$, $d=d_c/p_c=10$ nm, $g=p_c=0.68$; and for scaling, $\sigma_{dc}=2.6\times10^{17}$ sec^{-1}, $\epsilon_0=6.5$, $d=10$ nm, $p_c=0.68$, $A_1=A_2=1$, $A_3=A_4=0.75$, $C_0=0.5$, $\xi_0=10$ nm, $L_0=4$, $\mu=1.43$ (see Refs. 8 and 10). The sample-dependent parameters are

		EMT			Scaling				
Sample	p(TEM)	p	τ_0 (sec^{-1})	b_τ (sec)	p	τ_0 (sec^{1})	b_τ (sec)	$\bar{\xi}$ (μm)	λ_ξ (μm)
A	0.66		2×10^{-15}	2×10^{-16}	0.667	3×10^{-15}	1.5×10^{-16}	2	3590
B	0.74	0.715	2×10^{-16}	2×10^{-16}	0.74	3×10^{-15}	1.5×10^{-16}	0.25	10.6
C	0.80	0.79	7×10^{-15}	1.8×10^{-16}	0.80	6×10^{-15}	3.5×10^{-16}	0.1	0.82
D	0.84	0.84	6×10^{-15}	0.5×10^{-16}	0.84	6×10^{-15}	1.5×10^{-16}	0.07	0.3

where $\bar{\xi}=\xi_0\xi=\xi_0\Delta p^{-\nu}$, $\Delta p=(p-p_c)/p_c$, $\nu=\frac{4}{3}$, and λ_ξ is the optical wavelength at which $L(\omega)=\xi$, i.e., $\lambda_\xi=2\pi\xi_0(\bar{\xi}/\xi_0L_0)^{2+\theta}$.

[1]R. W. Cohen, G. D. Cody, M. D. Coutts, and B. Abeles, Phys. Rev. B **8**, 3689 (1973).
[2]J. C. Maxwell-Garnett, Philos. Trans. R. Soc. London **203**, 385 (1904).
[3]D. Bruggeman, Ann. Phys. (Leipzig) **24**, 6736 (1935).
[4]See, for example, C. G. Granqvist and O. Hunderi, Phys. Rev. B **16**, 3513 (1977); D. J. Bergman, *ibid.* **19**, 2359 (1979); P. Sheng, Phys. Rev. Lett. **45**, 60 (1980); T. Yamaguchi, M. Dgwawa, H. Takahashi, and N. Saito, Surf. Sci. **129**, 232 (1983); K. Driss-Khodja and S. Berthier, J. Phys. Condens. Matter 2, 8651 (1990).
[5]S. Norrman, T. Andersson, C. G. Granqvist, and O. Hunderi, Phys. Rev. B **18**, 674 (1978).
[6]P. Gadenne, Thin Solid Films **57**, 77 (1979).
[7]S. Berthier, J. Lafait, C. Sella, and Thran-Khanh-Vien, Thin Solid Films **125**, 171 (1985).
[8]Y. Yagil, M. Yosefin, D. J. Bergman, G. Deutscher, and P. Gadenne, Phys. Rev. B **43**, 11 342 (1991).
[9]Y. Gefen, A. Aharony, and S. Alexander, Phys. Rev. Lett. **50**, 77 (1983).
[10]P. Gadenne, Y. Yagil, and G. Deutscher, J. Appl. Phys. **66**, 3019 (1989).
[11]See, for example, D. E. Aspnes, *Optical Functions (Complex Refractive Index and Absorption), Properties of Silicon,* Inspec Data Review Series No. 4 (Inspec, London, 1988), and references therein.
[12]D. E. Aspnes and A. A. Stunda, Phys. Rev. B **27**, 985 (1983).
[13]G. Zachmann (unpublished).
[14]P. R. Griffiths and J. A. de Haseth, *Fourier Transform Infrared Spectroscopy* (Wiley, New York, 1986).
[15]C. Julien, in *Microionics—Solid State Integrable Batteries,* edited by M. Balkanski (Elsevier, New York, 1991), Chap. 2.5, p. 197.
[16]L. Genzel, H. R. Chandrasekhar, and J. Kuhl, Opt. Commun. **18**, 381 (1976).
[17]L. Genzel and K. Skar, J. Opt. Soc. Am. **67**, 871 (1977).
[18]Y. Yagil and G. Deutscher, Thin Solid Films **152**, 465 (1987).
[19]P. Gadenne, A. Beghdadi, and J. Lafait, Opt. Commun. **65**, 17 (1988).
[20]P. Gadenne, thése d'état, Université Paris VI, 1986.
[21]M.Kunz, G. A. Niklasson, and C. G. Granqvist, J. Appl. Phys. **64**, 3740 (1988).
[22]K. A. Khan, G. A. Niklasson, and C. G. Granqvist, J. Appl. Phys. **64**, 3327 (1988).
[23]T. S. Moss, *Optical Properties of Semi-Conductors* (Butterworths, London, 1961), p. 122.
[24]M. L. Theye, Phys. Rev. B **2**, 3060 (1970).
[25]J. P. Straley, J. Phys. C **9**, 783 (1976).

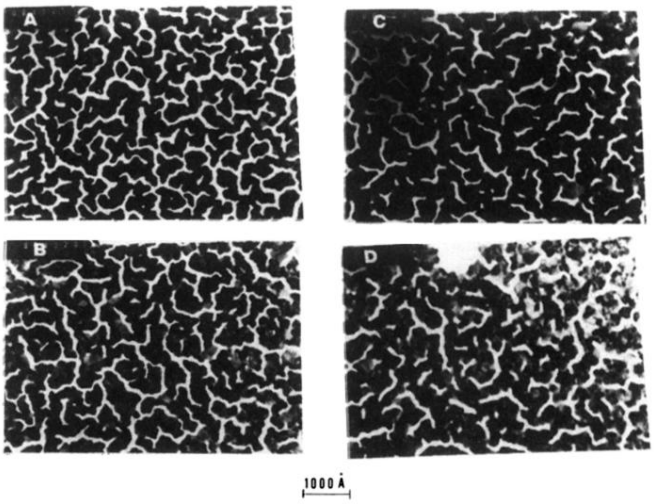

FIG. 2. TEM micrographs of samples $A-D$.